Dynamically Reconfigurable High Impedance and Frequency Selective Metasurfaces Using Piezoelectric Actuators

Marina Mavridou and Alexandros P. Feresidis, *Senior Member, IEEE*

Abstract—Novel dynamically reconfigurable low-loss high impedance and frequency selective metasurfaces (FSmSs) are presented, operating at around 15 GHz and incorporating compact piezoelectric actuators. The high impedance metasurface (HIS) consists of an array of metallic elements printed on a thin dielectric substrate, placed over a ground plane, and supported by the actuators. Under a dc bias, the actuators produce a displacement between the two layers, resulting in a change in the reflection phase response. Furthermore, novel multilayer FSmSs are proposed achieving significant tuning of their passband response with low losses. The FSmSs consist of three closely spaced periodic arrays of subwavelength nonresonant elements, namely, an array of metallic square loops placed between two arrays of square apertures in metallic sheets, separated by air cavities. The combination of the square loop array and one of the square aperture arrays produces a high impedance surface response, which is tuned using the piezoelectric actuators. This in turn alters the resonance condition of the complete FSmS structure and thus the central frequency of the passband. The structures have been investigated through simulations and measurements with good agreement, achieving an experimental frequency tuning range of 17% for the HIS and of 8.8% for the FSmS as well as a maximum phase shift of over 177° for the HIS at approximately 14 GHz.

Index Terms—Frequency selective surfaces (FSSs), high impedance surfaces (HIS), piezoelectric actuators, reconfiguration.

I. INTRODUCTION

METASURFACES are typically 2-D metamaterial structures [1], [2] formed by periodic arrays of metallic elements printed on dielectric substrates or apertures etched off metallic sheets. A periodic surface can be characterized as a metasurface if it consists of unit cells with subwavelength dimensions and exhibits extraordinary electromagnetic properties. Metasurfaces have been extensively investigated due to their properties such as negative [3] or near-zero refractive index [4], cloaking [5], anomalous reflection [6], focusing [7], and other applications.

A useful electromagnetic property that can be obtained from metasurfaces is an engineered reflection phase for impinging

The authors are with the School of Electronic, Electrical and Systems Engineering, University of Birmingham, Birmingham, B15 2TT, U.K. (e-mail: mmairin@hotmail.com; a.feresidis@bham.ac.uk).

electromagnetic waves. This is typically achieved when the periodic array is printed on a grounded dielectric substrate or placed at close proximity over a ground plane [8]–[11]. This type of metasurfaces which were introduced in [8], are called high impedance surfaces (HIS). For a specific frequency they exhibit a reflection phase of zero, acting as artificial magnetic conductors (AMCs). This characteristic makes them eligible for numerous applications such as ground planes in printed antennas [8] or in resonant cavity antennas for reducing their profile [9], [10]. Other applications of HIS type structures include reflectarrays [12], polarization converters [13], and holographic surfaces [14]. Furthermore, several tunable HIS structures have been proposed in the past few years using active components such as varactor diodes [15]–[17]. These components have been successfully employed for applications at low microwave frequencies, but are not suitable for higher frequencies mainly due to high losses and parasitic effects. Moreover tunable HIS surfaces acting as reflectarrays have been proposed for mm-wave and sub-mm-wave frequencies based on microelectromechanical systems (MEMS) [18], [19] and liquid crystals [20], respectively. A more detailed overview of tuning techniques for HIS or reflectarray type structures including a qualitative comparison of the technologies is given in [21]. More recently, the use of linear piezoelectric actuators has been proposed for the dynamic control of a HIS operated as a phase shifting surface at frequencies around 60 GHz [22]. However, linear piezoactuators achieve only a very limited displacement which is only useful toward the high end of the mm-wave band.

Frequency selective surfaces (FSSs) have attracted a lot of interest over the past decades for their filtering properties [23]–[30]. They typically consist of elements with larger unit cell dimensions compared to metasurfaces and exhibit total reflection (conducting element) or total transmission (aperture elements) at their resonance frequency [23], [24]. A number of element geometries have been investigated such as dipole, square or circular patches or apertures. Additionally, convoluted elements, such as spirals or more complicated geometries have been reported for miniaturization purposes. Still, the operation of these designs is based on the elements' resonance. Thus, in order to obtain tuning of an FSS response, a change on the effective size of the element has to be performed. This has been achieved by introducing varactor [25] or PIN diodes [26] on each element for low frequency applications, or MEMS [27], [28] and ferroelectric varactors [29] for mm-wave frequencies. Moreover, tunable substrates have been employed, where by changing the permittivity of the substrate,
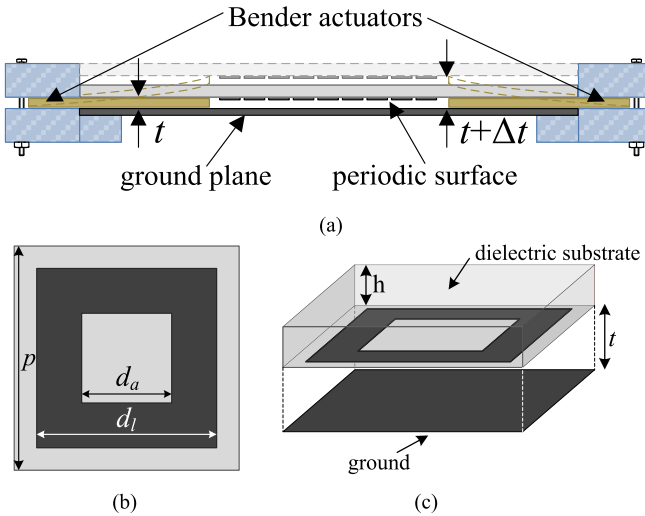
Fig. 1. (a) Proposed tunable HIS (dimensions are not to scale) and unit cell of the HIS array. (b) Top view. (c) Perspective.

the guided wavelength is changed resulting in a different operating frequency. Such tunable substrates can be ferroelectric substrates [30] for lower microwave frequencies which have the disadvantage of high losses, and liquid crystals which are suitable for higher mm-wave frequencies but also exhibit high losses and low switching speeds [31], [32].

In this paper, we present three main contributions to the design and implementation of dynamically tunable HIS and FSS structures:

First, a low-loss technique for tuning high impedance metasurfaces at lower mm-wave bands is presented and experimentally demonstrated. The tuning is achieved by virtue of employing a small number of piezoelectric bender actuators that can achieve a significantly higher displacement under a dc bias compared to previously reported linear piezoactuators. The high impedance metasurface (HIS) consists of an array of metallic elements printed on a thin dielectric substrate, placed over a ground plane, and supported by four actuators (Fig. 1). It is important to note that the actuators are placed around the HIS array, thereby not interfering with its radiation performance and hence resulting in a particularly low loss structure, which is especially challenging at mm-wave frequencies. A displacement is produced by the actuators when they are biased with a dc voltage, changing thus the distance between the HIS array and the ground and resulting in a change of the reflection phase response of the structure.

The second contribution of this paper is a novel design of multilayer frequency selective metasurfaces (FSmSs). In contrast to conventional FSS, the proposed FSmS consist of multiple layers of nonresonant subwavelength periodic metasurfaces. In particular, a periodic array of square loop elements is placed between two periodic arrays of square apertures on metallic sheets, separated by thin subwavelength air cavities (see Fig. 6). The combination of the square loop array and one of the square aperture arrays produces a HIS response. The overall passband response of the FSmS is produced by the resonance of the formed subwavelength cavities and not by the resonance of the elements of the arrays.

The third contribution of this paper is the dynamic tuning of the response of the proposed FSmS. This is achieved by tuning the HIS response using the actuators (by changing the distance between the two surfaces) which in turn alters the resonance condition of the complete structure and thus the central frequency of the passband of the proposed FSmS. The design and tunability of the proposed FSmS is presented. The angular stability is also studied and discussed. Simulation and measurement results are presented validating the proposed concept.

II. TUNABLE HIGH IMPEDANCE METASURFACE

The proposed high impedance metasurface shown in Fig. 1(a) consists of a doubly periodic array of square loop metallic elements [24], printed on a 0.055 mm thick dielectric substrate with $\varepsilon_r = 3$ and $\tan\delta = 0.0018$ placed at distance t from a ground plane. It should be pointed out here that the HIS performance is related to the resonance of an open cavity formed between the periodic array and the ground as explained in [11], resulting in a strong dependence of the reflection phase on the cavity distance t.

A. Design of Tunable HIS Structure

The unit cell of the proposed tunable HIS is shown in Fig. 1(b) and (c). The periodicity of the structure is $p = 6.5$ mm, the outer dimension of the square loop is $d_l = 5.57$ mm, the inner square loop dimension is $d_a = 3.34$ mm and the initial cavity thickness is set to $t = 0.6$ mm. The dimensions and the geometry of the structure have been chosen so that a reflection phase of zero is obtained at around 15 GHz with a fast variation of the reflection phase with frequency which makes the structure more sensitive to changes of the cavity distance [11]. The periodic surface is supported by four piezoelectric actuators placed at the four corners. A change in the biasing voltage of the bender actuators is translated to a bending of the actuators and thus a vertical displacement of the surface with respect to the ground plane [Fig. 1(a)]. In order to evaluate the tuning range and the maximum phase shift that can be achieved from the proposed HIS, simulations have been carried out in CST Microwave Studio simulation software. The displacement achieved by the bender actuators is modeled in the software as a parametric change of the cavity thickness t.

Periodic boundary conditions have been employed to reduce the calculations of an infinite structure into a single unit cell and full wave analysis has been carried out in CST with normally incident plane wave excitation to extract its reflection characteristics. The simulated phase of the reflection coefficient is shown in Fig. 2(b) for different cavity distances which correspond to a displacement from zero ($t = 0.6$ mm) to 1.6 mm ($t = 2.2$ mm). The corresponding reflection magnitude is shown in Fig. 2(a). For a displacement Δt of just 0.4 mm, a 142° phase shift has been obtained for operation at 15 GHz while for $\Delta t = 1.6$ mm the obtained phase shift at the same frequency is about 190°. The maximum phase shift for this displacement is 243° at 13.46 GHz [Fig. 2(c)]. Furthermore, the frequency where the AMC response occurs, i.e., where the reflection phase is equal to zero, is tuned from 15.53 to 10.85 GHz for $\Delta t = 1.6$ mm. It is worth noting that as

(a)

(b)

Fig. 3.   (a) Schematic of piezoelectric bender actuator. (b) Photograph of commercial piezoelectric actuator.

cavity thickness of the HIS. Therefore, the maximum tuning range of the structure depends on the maximum displacement produced by the actuators. The bender actuators proposed for this application are built from two layers of ceramic plates placed on top of each other [Fig. 3(a)]. Each ceramic layer has the property of expanding or contracting when exposed to positive or negative electrical potential, respectively, due to the inverse piezoelectric phenomenon. Different voltages are applied to the upper and lower layer through the three electrodes ($+$V, 0, $-$V) provoking an expansion to the upper layer and a contraction to the lower one. This phenomenon creates a bending of the actuator, similar to the principle of thermostatic bimetals that translate the small change in the length of the ceramic plates into a large vertical displacement [Fig. 1(a)]. The total displacement of a piezoelectric bender actuator depends on its total length. The proposed actuators have a quick time response in the order of milliseconds and can achieve displacements up to several millimeters with a blocking force of up to a few newtons [33]. In the proposed design, the actuators that have been employed are the commercial actuators PL140.11 from Physik Instrumente [Fig. 3(b)]. They are 45 mm long, 11 mm wide and 0.6 mm thick and can achieve a maximum displacement of 1 mm for a biasing voltage of 60 V with a nominal error of $\pm 20\%$.

C. Fabrication and Measurements

A prototype of the proposed structure has been fabricated and tested to validate the simulation results. A periodic array of 38×38 copper square loop elements printed on a 0.055 mm thick, polyester film ($\varepsilon_r = 3$) with overall dimensions 240 mm $\times$ 240 mm ($\sim 12\lambda \times 12\lambda$) has been used for the measurement (Fig. 4). The periodic surface has been glued to polystyrene foam ($\varepsilon_r \approx 1$) to make it rigid while keeping it lightweight, and then positioned on top of the ground plane supported by the piezoelectric actuators. In this experimental configuration, for simplicity, the periodic surface is merely supported by the actuators in a horizontal position. However, well known mechanical techniques can be applied to provide a more robust supporting structure with the actuators. Based on the above, the initial cavity distance has been set from the thickness of the actuators (~ 0.6 mm)
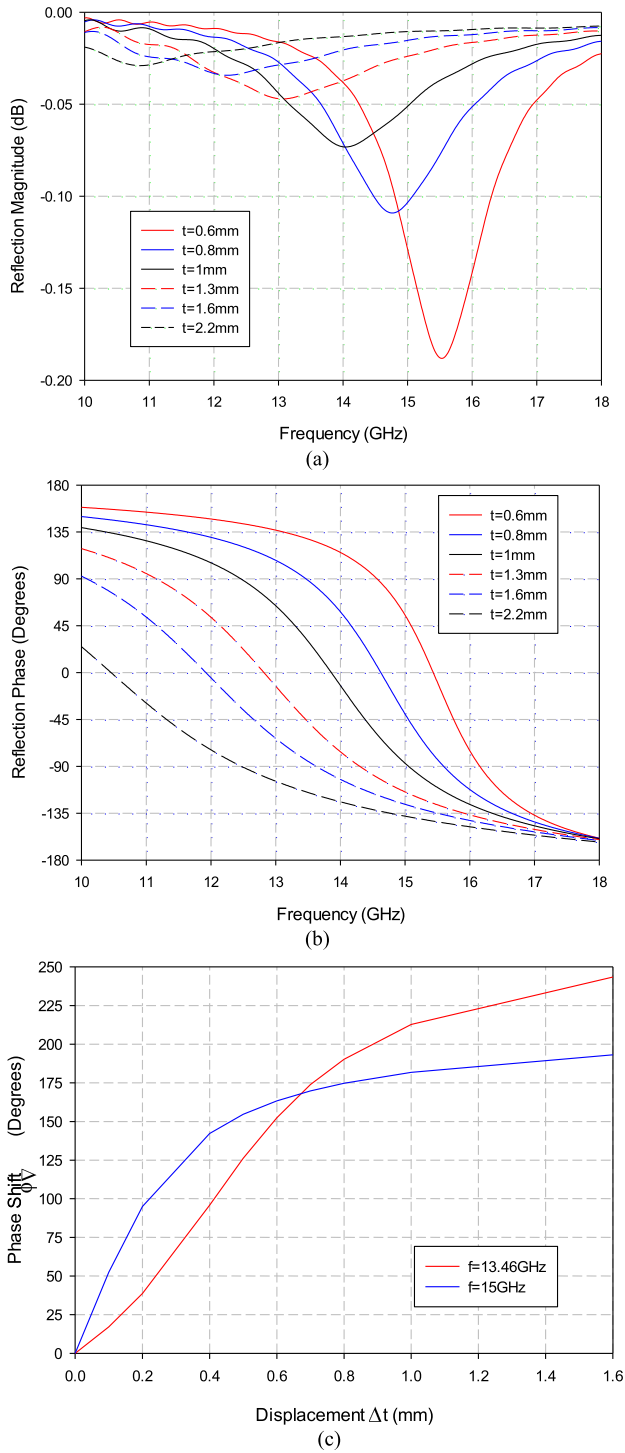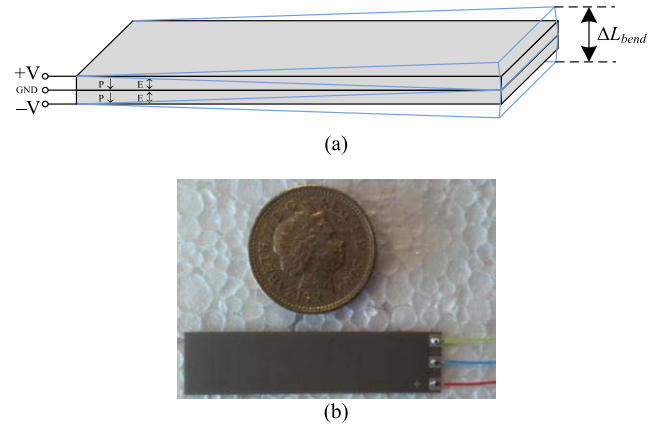

(a)

(b)

(c)

Fig. 2.   Simulated reflection. (a) Magnitude and (b) phase of the proposed HIS for different cavity thicknesses. (c) Phase shift versus displacement for $f = 13.46$ and 15 GHz.

the cavity thickness increases, the HIS resonance is weaker and the slope in the reflection phase is decreased [11]. This results in a nonlinear tuning of the phase response. This is shown more clearly in Fig. 2(c) where the phase shift $\Delta\varphi$ versus the displacement Δt is depicted for frequencies 13.46 and 15 GHz.

B. Piezoelectric Bender Actuators

The tuning concept in this paper is based on the use of piezoelectric bender actuators that dynamically change the
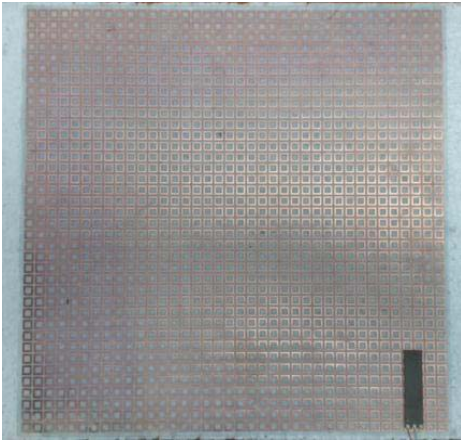
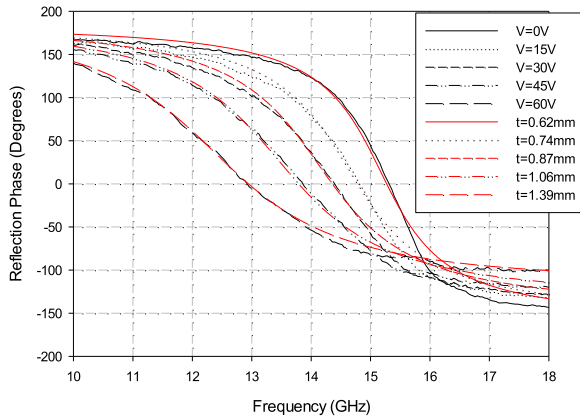Fig. 4. Photograph of the fabricated periodic surface and actuator.

Fig. 5. Measured reflection phase for different voltages compared to simulated results.

and has then increased by applying voltage to the electrodes. Two horn antennas have been used to measure the reflection characteristics of the proposed HIS, one as a transmitter and one as a receiver, aiming the structure under test with a small angle of incidence/reflection. The measured reflection phase for biasing voltages $V = 0$–60 V is presented in Fig. 5. Significant tuning has been achieved with the AMC (zero phase) frequency shifting from 15.32 GHz to slightly less than 13 GHz ($\sim$17% tuning range). In addition a significant phase shift ($\Delta\varphi$) has been obtained from the proposed tunable HIS with the maximum $\Delta\varphi$ of 177.4° observed at about 14 GHz. The corresponding magnitude is not shown here, since due to the very low losses of the structure, there was no prominent resonance but just a 0.5 dB ripple below zero over the measured frequency range caused by standing wave reflections during the measurement. Although the concept of the proposed design has been validated from the measurements, a comparison with the simulated performance (also included in Fig. 5) has shown that the actual displacement that has been achieved from the actuators was about 0.8 mm instead of 1 mm, which is within the initial expected error of the supplied actuators.

III. TUNABLE FREQUENCY SELECTIVE METASURFACES

In this section, a tunable FSmS structure is designed, having as a starting point the HIS described in Section II. The unit cell of the FSmS is shown in Fig. 6(a). The main feature of the proposed FSmS design is that its operation
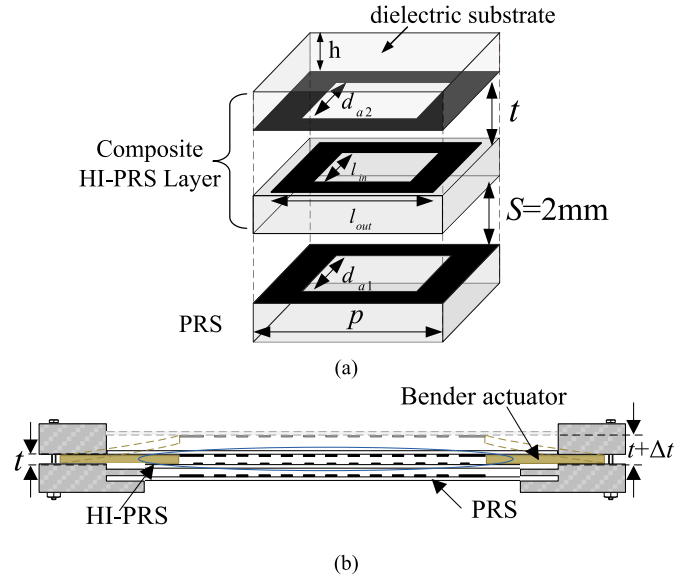

Fig. 6. (a) Unit cell of the multilayer FSmS. (b) Schematic of proposed tunable FSmS structure (dimensions are not to scale).

is based on a resonant cavity effect, and not the resonance of the periodic array elements (which are of subwavelength dimensions). It is well known that a Fabry–Perot type resonant cavity can be typically obtained from two highly reflective periodic arrays acting as partially reflective surfaces (PRSs), i.e., FSSs operated at frequencies away from their resonance, placed at approximately half-wavelength distance from each other [34]. This resonant cavity normally produces a passband response.

In this paper, however, one of the PRSs is replaced by a composite double layer structure described in Section III-A, acting both as a PRS and a HIS. This composite structure will be referred to as high impedance PRS (HI-PRS) and it consists of an array of square loop metallic patches printed on a thin substrate and an array of square apertures on a metallic sheet printed on the same type and thickness substrate [Fig. 6(a)]. The two surfaces are separated by a subwavelength air cavity t. The proposed FSmS is formed by placing another PRS at a distance S from the HI-PRS [Fig. 6(a) and (b)]. Due to the reflection phase values of the HI-PRS, a significant reduction of the cavity thickness S and therefore the overall profile of the FSmS is achieved as explained in Section III-B. Tuning of the passband response is obtained by changing the HI-PRS cavity t using the bender actuators which alters the reflection phase and consequently the resonant condition.

A. Design of High Impedance Partially Reflective Surface

It is well known that in order to obtain a HIS response, a periodic surface has to be placed at close proximity to a ground plane or to be printed on a grounded substrate. At such structures no transmission occurs, and total reflection of the incident waves takes place. However, it has been shown in recent works [35] that if the ground plane is replaced with a nonresonant aperture array (inductive surface), the high impedance response is maintained, while obtaining a partial transmission/reflection of incident waves.
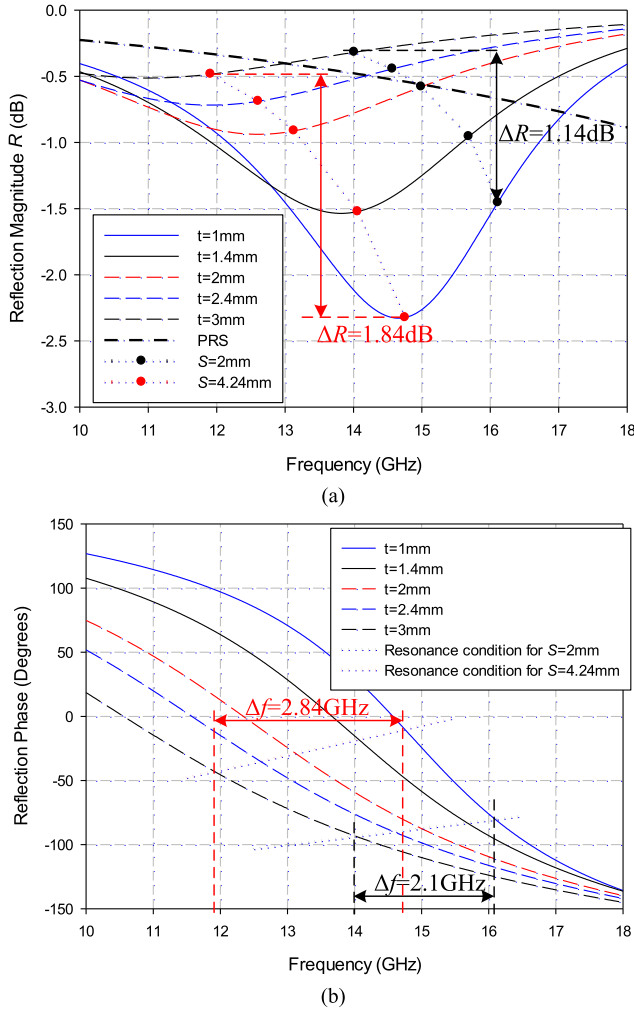
Fig. 7. Simulated reflection (a) magnitude and (b) phase of the HI-PRS for different cavity distances t.

Fig. 8. Simulated (a) transmission and (b) reflection of the proposed tunable FSmS for different cavity distances t (keeping $S = 2$ mm).

Based on the above, the HI-PRS has been designed starting from the HIS of Section II. A square loop array is printed on a thin dielectric substrate with thickness $h = 0.055$ mm and $\varepsilon_r = 3$. The periodicity of the structure and the dimensions of the square loop element are $p = 7$ mm, $l_{out} = 5$ mm, and $l_{in} = 3.5$ mm [see Fig. 6(a)] which are slightly modified compared to the HIS dimensions of Section II. Moreover, the ground plane is replaced with a square aperture array of the same periodicity ($p = 7$ mm) and aperture size $d_{a2} = 4.5$ mm. The array is printed on the same type and thickness substrate and placed over the square loop array at a distance t as shown in Fig. 6.

The structure has been simulated in CST for different cavity distances t from 1 to 3 mm and the extracted reflection coefficients are depicted in Fig. 7. It can be seen from the magnitude of the reflection coefficient [Fig. 7(a)] that a partial reflection is obtained, while a high impedance operation in terms of the reflection phase is achieved for operation between approximately 10 and 15 GHz for the particular cavity thicknesses [Fig. 7(b)]. In Fig. 7(a), it is shown that the minimum of the reflection magnitude becomes less prominent as the cavity thickness increases corresponding to higher reflection and reduced transmission of the incident plane wave. Moreover,
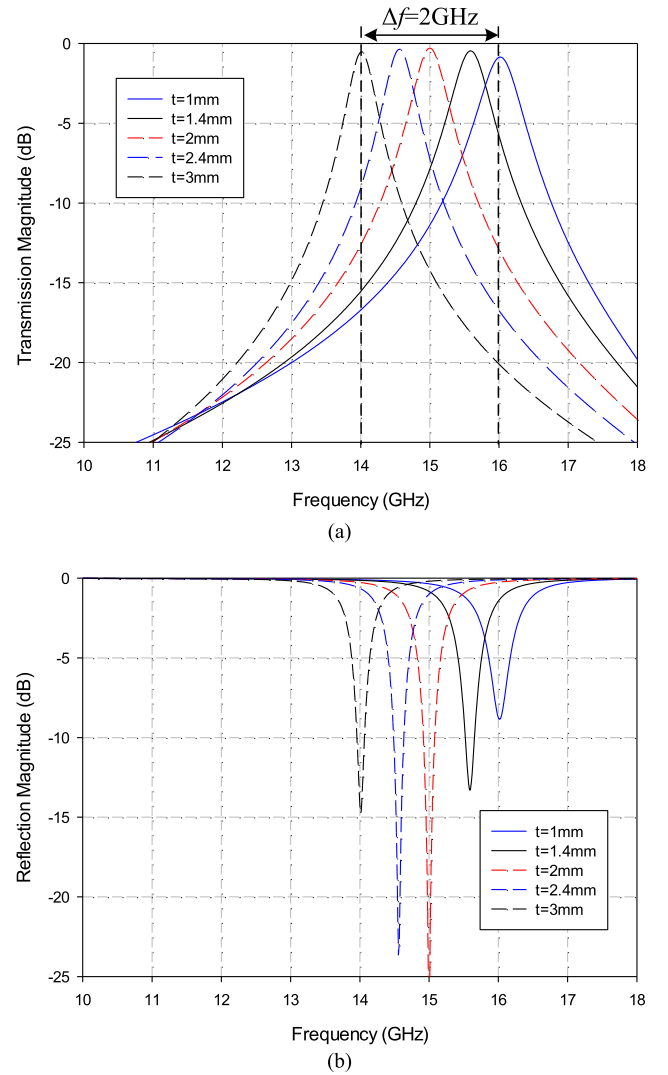
Fig. 7(b) shows a decreased slope of the reflection phase for increased cavity thickness.

B. Frequency Selective Metasurfaces Based on High Impedance PRS

The HI-PRS described in the previous subsection is subsequently employed to create the proposed FSmS (Fig. 6). The square aperture PRS placed at distance S below the HI-PRS has periodicity equal to the periodicity of the HI-PRS array ($p = 7$ mm), while the size of the aperture is $d_{a1} = 4.5$ mm. As explained earlier, the concept of the proposed FSmS is based on a cavity type resonance, which is obtained by satisfying the resonance condition

$$\phi_{\text{HI-PRS}} + \phi_{\text{PRS}} - \frac{2\pi}{\lambda} 2S = \pm 2N\pi, \quad N = 0, 1, 2 \dots \quad (1)$$

where $\varphi_{\text{HI-PRS}}$ is the reflection phase of the HI-PRS, φ_{PRS} the reflection phase of the PRS, and λ the wavelength. For operation at 16.11 GHz, substituting the reflection phase of the HI-PRS for $t = 1$ mm which is $\varphi_{\text{HI-PRS}} = -80.88°$ [Fig. 7(b)] and the reflection phase of the PRS which is $\varphi_{\text{PRS}} = 157.81°$ in (1), the cavity distance should be $S = 2$ mm. Indeed,
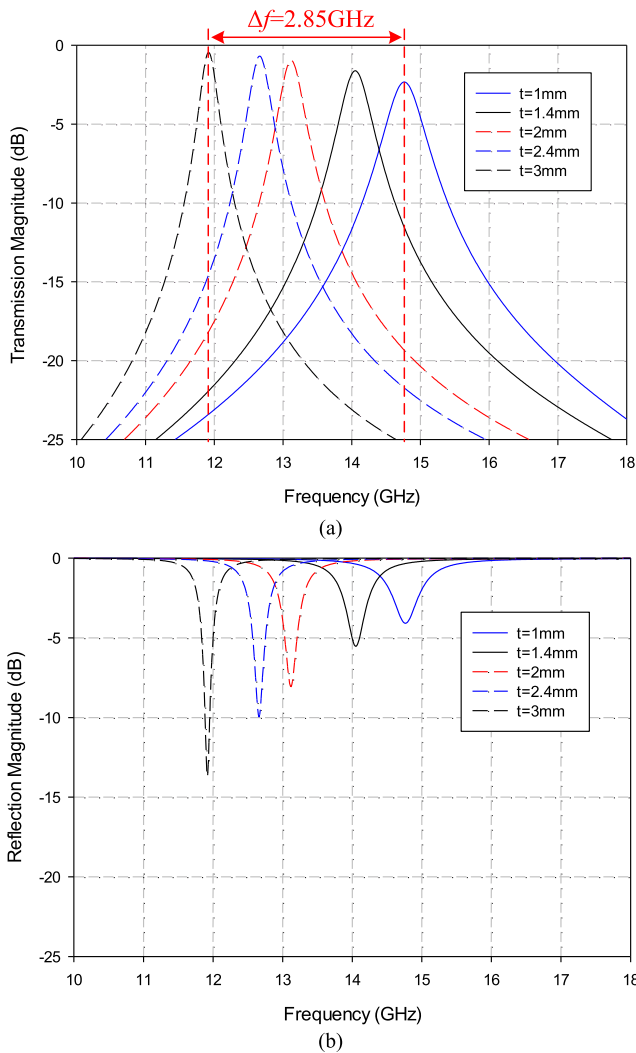
Fig. 9. Simulated (a) transmission and (b) reflection response for alternative design with $S = 4.24$ mm for different HI-PRS cavities.

Fig. 10. Angular stability study for the proposed tunable FSmS with $S = 2$ mm, and the design with $S = 4.24$ mm (t = 1 mm).

from the simulated transmission coefficient magnitude of the proposed FSmS for $t = 1$ mm and $S = 2$ mm shown in Fig. 8(a), a passband is observed at $f = 16$ GHz which is very close to the calculated operational frequency from the theoretical analysis.

By employing the same tuning technique as in the case of the tunable HIS of Section II, the reflection phase of the HI-PRS can be tuned. This is achieved using bender actuators to increase the cavity distance t by displacing the upper layer of the composite structure, as illustrated in Fig. 6(b). It is expected that if the cavity distance S between the PRS and the HI-PRS is kept constant, then the resonance condition (1) will be satisfied for lower frequencies as t increases and tuning of the passband will be obtained. This can be demonstrated from the black dotted line in Fig. 7(b) which shows the ideal phase for the HI-PRS that satisfies the resonant condition (1). The points where the dotted line intersects the simulated reflection phase define the expected tuning range which as can be seen from the figure is 2.1 GHz for displacement from $t = 1$ mm to $t = 3$ mm. Indeed, the transmission response of the proposed tunable FSmS for t between 1 and 3 mm is presented in Fig. 8(a) and shows a tuning of the passband from
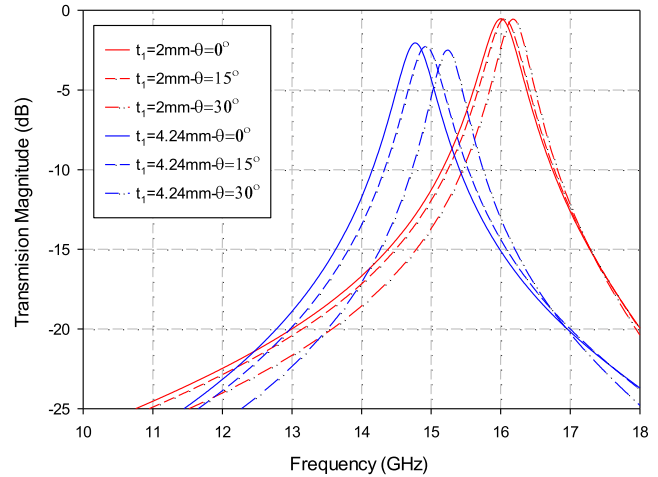
16 to 14 GHz, which is only slightly less than that expected from the theoretical analysis. Moreover, it can be observed that the insertion loss is between 0.28 dB ($t = 2$ mm) and 0.85 dB ($t = 1$ mm). The corresponding reflection magnitude of the structure is also shown in Fig. 8(b). The reflection magnitude is below -10 dB for all cavity distances, except from $t = 1$ mm where it is slightly higher than -10 dB.

The slightly increased insertion loss at the extreme cases of $t = 3$ mm and more significantly $t = 1$ mm is attributed to mismatch effects and becomes more pronounced in the following case. If the HI-PRS is operated close to the AMC frequency, and more specifically where the reflection phase is $\varphi_{\text{HI-PRS}} = -10°$, then from (1) the cavity thickness S becomes equal to 4.24 mm. For this case, the ideal reflection phase $\varphi_{\text{HI-PRS}}$ versus frequency is presented in Fig. 7(b) with the red dotted line. Consequently, the estimated tuning range of an alternative FSmS structure with $S = 4.24$ mm can be extracted again from the intersection points of the ideal phase with the reflection phase for $t = 1$ mm and $t = 3$ mm. Therefore, as can be seen from the figure, the expected tuning range is $\Delta f = 2.84$ GHz which is larger than the one obtained from the design with $S = 2$ mm. This is also shown from the transmission response of the new structure for $t = 1$ mm to $t = 3$ mm [Fig. 9(a)], with the passband tuned from 14.77 to 11.92 GHz ($\Delta f = 2.85$ GHz). This increase in the tuning range of this particular alternative structure is expected, since as we move toward the point where the reflection phase is zero, the phase curves for different cavity distances t tend to exhibit higher spectral separation, whereas at higher frequencies the phase curves tend to converge [Fig. 7(b)].

However, although the last design has the advantage of a larger tuning range compared to the first design, it exhibits worse performance in terms of the insertion loss, particularly for small values of t. This is evident from the transmission coefficient as well as the reflection coefficient response of the structure [Fig. 9(b)]. The latter is below -10 dB only for the case of $t = 3$ mm while the insertion loss is 2.33 dB for $t = 1$ mm. This effect is related to the resonant cavity nature of the structure. Such structures should have similar reflectivities between the layers forming the cavity in order to

avoid impedance mismatch, which causes increased insertion loss [34]. So, a better explanation of the observed insertion loss can be obtained from Fig. 7(a), showing the reflection magnitude R of the PRS, as well as the values of R of the two alternative HI-PRS designs at each operating frequency (corresponding to the different cavity distances t) with the dotted lines. It can be observed that the reflection magnitude of the HI-PRS with $S = 4.24$ mm (red dotted line) exhibits a large variation for $t = 1$ mm to $t = 3$ mm with respect to that of the PRS. In contrast, in the case of the proposed HI-PRS with $S = 2$ mm (black dotted line) the total variation of the reflection magnitude is significantly less ($\Delta R = 1.14$ dB as opposed to 1.84 dB for the case of $S = 4.24$ mm) and follows closer the reflection magnitude of the PRS, resulting in better performance in terms of insertion loss.

Another reason for choosing the design with $S = 2$ mm is the reduced total profile varying from $\lambda/6$ for $t = 1$ mm to $\lambda/4$ for $t = 3$ mm, while for the case of $S = 4.24$ mm the profile is at least $\lambda/3$. This thinner profile results in a more angularly stable structure, which is evident from Fig. 10. In particular, the figure shows the transmission response for $t = 1$ mm for both designs with angles of incidence from 0° to 30°. It can be seen that the proposed structure exhibits a very small shift (1.1%) while the design with $S = 4.24$ mm undergoes a shift from 14.77 to 15.24 GHz (3.1%). Finally, the proposed concept can be extended to even thinner cavities with optimized HI-PRS and PRS which will provide even better angular stability. Finally the tunable performance of the proposed structure can be used in order to provide angularly stable responses for even higher angles of incidence.

C. Measurements of Fabricated Prototype

Finally, a prototype of the proposed tunable FSmS has been fabricated in order to experimentally validate the concept. Three periodic arrays of 35×35 elements have been fabricated, two arrays of square apertures etched off a copper sheet and one array of square loop copper elements. Each of the arrays was printed on thin polyester films with $\varepsilon_r = 3$, $\tan\delta = 0.03$, thickness 0.055 mm and overall dimensions 250 mm×250 mm ($12.5\lambda \times 12.5\lambda$). To facilitate the measurement set up and define the fixed distance $S = 2$ mm, the PRS array has been glued on a 2 mm thick Rohacell-51 substrate ($\varepsilon_r \approx 1$). The square loop array has been glued to the other side of the Rohacell-51 substrate, carefully aligning the two arrays. Subsequently, spacers of 1.1 mm thickness where placed around the square loop array where the bender actuators have been positioned. Finally, the other square aperture array (forming the upper layer of the composite HI-PRS) has been glued to polystyrene foam to make it rigid and placed on top, supported by the actuators. Two horn antennas were used for the measurement of the transmission characteristics of the fabricated prototype for different voltages applied to the actuators. The measured transmission response in comparison with the corresponding simulated results is shown in Fig. 11. Good agreement has been obtained with an achieved tuning of 8.8% for $\Delta t = 1.2$ mm. Moreover, a dynamic range of more than 20 dB at 15.3 GHz has been achieved for voltages 0 and 60 V, demonstrating that the proposed FSmS
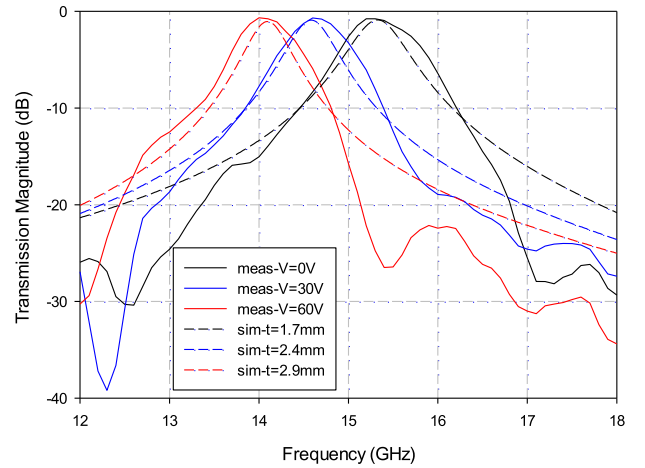

Fig. 11. Measured transmission magnitude for different voltages and comparison with simulated results.

TABLE I
COMPARISON OF SELECTED TUNABLE FSS TECHNOLOGIES

Technology [Ref]	Freq [GHz]	Insertion Loss (Min) [dB]	Insertion Loss (Max) [dB]	Tuning range (%)	Switch Speed
This work	14.7	0.3	0.8	8.8%	~ msec
Liquid Crystal [32]	27.1	6.2±0.7	6.2±0.7	2%	>20msec
MEMS [27]	30	2	2.9	2.7%	~ 10 μsec
Ferroelectric [29]	12	2.5	3	10%	~ sub-μsec

can be tuned from a transmitting to a reflecting structure. It should be pointed out at this point that the actuators used for this measurement produced a displacement of 1.2 mm which is within the ±20% of manufacturing error. Table I shows a comparison of the major tuning parameters between our proposed technology and other recently reported technologies for tunable FSS over 10 GHz. The proposed technology in this paper exhibits very low losses compared to other techniques and very good tuning performance.

IV. CONCLUSION

Dynamically tunable low-loss high impedance and FSmSs based on piezoelectric bender actuators have been demonstrated through simulation and experiments. Initially a HIS has been designed and measured giving a phase shift of 177.4° at 14 GHz. Subsequently, a new type of FSS has been presented based on multilayer metasurfaces achieving a measured tuning of the passband of 8.8% for operation around 14.7 GHz. Both structures exhibit very low loss performance. The proposed structures and tuning technique are directly scalable to higher mm-wave frequencies paving the way for a new class of low-loss tunable mm-wave FSS and related structures.

REFERENCES

[1] F. Falcone *et al.*, "Babinet principle applied to the design of metasurfaces and metamaterials," *Phys. Rev. Lett.*, vol. 93, pp. 1974011–1974014, Nov. 2004.

[2] N. Yu and F. Capasso, "Flat optics with designer metasurfaces," *Nature Mater.*, vol. 13, pp. 139–150, Jan. 2014.

[3] A. V. Kildishev, A. Boltasseva, and V. M. Shalaev, "Planar photonics with metasurfaces," *Science*, vol. 339, no. 6125, p. 1232009, Mar. 2013.

[4] G. D'Aguanno, N. Mattiucci, M. J. Bloemer, R. Trimm, N. Aközbek, and A. Alù, "Frozen light in a near-zero index metasurface," *Phys. Rev. B*, vol. 90, no. 5, p. 054202, 2014.

[5] Y. Chen and A. Alù, "Mantle cloaking using thin patterned metasurfaces," *Phys. Rev. B*, vol. 84, p. 205110, Nov. 2011.

[6] N. M. Estakhri and A. Alù, "Manipulating optical reflections using engineered nanoscale metasurfaces," *Phys. Rev. B*, vol. 89, no. 23, p. 235419, Jun. 2014.

[7] R. Fleury, D. L. Sounas, and A. Alù, "Negative refraction and planar focusing based on parity-time symmetric metasurfaces," *Phys. Rev. Lett.*, vol. 113, no. 2, p. 023903, Jul. 2014.

[8] D. Sievenpiper, L. Zhang, R. F. J. Broas, N. G. Alexopolous, and E. Yablonovitch, "High-impedance electromagnetic surfaces with a forbidden frequency band," *IEEE Trans. Microw. Theory Techn.*, vol. 47, no. 11, pp. 2059–2074, Nov. 1999.

[9] S. Wang, A. P. Feresidis, G. Goussetis, and J. C. Vardaxoglou, "Low-profile resonant cavity antenna with artificial magnetic conductor ground plane," *Electron. Lett.*, vol. 40, no. 7, pp. 405–406, Apr. 2004.

[10] A. P. Feresidis, G. Goussetis, S. Wang, and J. C. Vardaxoglou, "Artificial magnetic conductor surfaces and their application to low-profile high-gain planar antennas," *IEEE Trans. Antennas Propag.*, vol. 53, no. 1, pp. 209–215, Jan. 2005.

[11] G. Goussetis, A. P. Feresidis, and J. C. Vardaxoglou, "Tailoring the AMC and EBG characteristics of periodic metallic arrays printed on grounded dielectric substrate," *IEEE Trans. Antennas Propag.*, vol. 54, no. 1, pp. 82–89, Jan. 2006.

[12] J. Huang and J. A. Encinar, *Reflectarray Antennas*. Hoboken, NJ, USA: Wiley, 2008.

[13] E. Doumanis, G. Goussetis, J. L. Gomez-Tornero, R. Cahill, and V. Fusco, "Anisotropic impedance surfaces for linear to circular polarization conversion," *IEEE Trans. Antennas Propag.*, vol. 60, no. 1, pp. 212–219, Jan. 2012.

[14] B. H. Fong, J. S. Colburn, J. J. Ottusch, J. L. Visher, and D. F. Sievenpiper, "Scalar and tensor holographic artificial impedance surfaces," *IEEE Trans. Antennas Propag.*, vol. 58, no. 10, pp. 3212–3221, Oct. 2010.

[15] C. Mias and J. H. Yap, "A varactor-tunable high impedance surface with a resistive-lumped-element biasing grid," *IEEE Trans. Antennas Propag.*, vol. 55, no. 7, pp. 1955–1962, Jul. 2007.

[16] F. Costa, A. Monorchio, S. Talarico, and F. M. Valeri, "An active high-impedance surface for low-profile tunable and steerable antennas," *IEEE Antennas Wireless Propag. Lett.*, vol. 7, pp. 676–680, 2008.

[17] R. Guzman-Quiros, J. L. Gomez-Tornero, A. R. Weily, and Y. J. Guo, "Electronically steerable 1-D Fabry–Perot leaky-wave antenna employing a tunable high impedance surface," *IEEE Trans. Antennas Propag.*, vol. 60, no. 11, pp. 5046–5055, Nov. 2012.

[18] O. Bayraktar, O. A. Civi, and T. Akin, "Beam switching reflectarray monolithically integrated with RF MEMS switches," *IEEE Trans. Antennas Propag.*, vol. 60, no. 2, pp. 854–862, Feb. 2012.

[19] C. Guclu, J. Perruisseau-Carrier, and O. Civi, "Proof of concept of a dual-band circularly-polarized RF MEMS beam-switching reflectarray," *IEEE Trans. Antennas Propag.*, vol. 60, no. 11, pp. 5451–5455, Nov. 2012.

[20] G. Perez-Palomino *et al.*, "Design and experimental validation of liquid crystal-based reconfigurable reflectarray elements with improved bandwidth in f-band," *IEEE Trans. Antennas Propag.*, vol. 61, no. 4, pp. 1704–1713, Apr. 2013.

[21] S. V. Hum and J. Perruisseau-Carrier, "Reconfigurable reflectarrays and array lenses for dynamic antenna beam control: A review," *IEEE Trans. Antennas Propag.*, vol. 62, no. 1, pp. 183–198, Jan. 2014.

[22] M. Mavridou, A. P. Feresidis, P. Gardner, and P. S. Hall, "Tunable millimetre-wave phase shifting surfaces using piezoelectric actuators," *IET Microw. Antennas Propag.*, vol. 8, no. 11, pp. 829–834, Aug. 2014.

[23] R. Mittra, C. H. Chan, and T. Cwik, "Techniques for analyzing frequency selective surfaces-a review," *Proc. IEEE*, vol. 76, no. 12, pp. 593–615, Dec. 1988.

[24] B. A. Munk, *Frequency Selective Surfaces: Theory and Design*. Hoboken, NJ, USA: Wiley, 2000.

[25] C. Mias, "Varactor-tunable frequency selective surface with resistive-lumped-element biasing grids," *IEEE Microw. Wireless Compon. Lett.*, vol. 15, no. 9, pp. 570–572, Sep. 2005.

[26] B. Sanz-Izquierdo, E. A. Parker, and J. C. Batchelor, "Switchable frequency selective slot arrays," *IEEE Trans. Antennas Propag.*, vol. 59, no. 7, pp. 2728–2731, Jul. 2011.

[27] B. Schoenlinner, A. Abbaspour-Tamijani, L. C. Kempel, and G. M. Rebeiz, "Switchable low-loss RF MEMS Ka-band frequency-selective surface," *IEEE Trans. Microw. Theory Techn.*, vol. 52, no. 11, pp. 2474–2481, Nov. 2004.

[28] J. M. Zendejas, J. P. Gianvittorio, Y. Rahmat-Samii, and J. W. Judy, "Magnetic MEMS reconfigurable frequency-selective surfaces," *J. Microelectromech. Syst.*, vol. 15, no. 3, pp. 613–623, Jun. 2006.

[29] M. Sazegar *et al.*, "Beam steering transmitarray using tunable frequency selective surface with integrated ferroelectric varactors," *IEEE Trans. Antennas Propag.*, vol. 60, no. 12, pp. 5690–5699, Dec. 2012.

[30] E. A. Parker and S. B. Savia, "Active frequency selective surfaces with ferroelectric substrates," *IEE Proc.-Microw. Antennas Propag.*, vol. 148, no. 2, pp. 103–108, Apr. 2001.

[31] W. Hu *et al.*, "Liquid crystal tunable mm wave frequency selective surface," *IEEE Microw. Wireless Compon. Lett.*, vol. 17, no. 9, pp. 667–669, Sep. 2007.

[32] N. Tentillier, F. Krasinski, R. Sauleau, B. Splingart, H. Lhermite, and P. Coquet, "A liquid-crystal, tunable, ultra-thin Fabry–Perot resonator in Ka band," *IEEE Antennas Wireless Propag. Lett.*, vol. 8, pp. 701–704, 2009.

[33] (Jun. 2015). *N/A*. [Online]. Available: http://www.physikinstrumente.co.uk

[34] A. C. D. Lima and E. A. Parker, "Fabry–Perot approach to the design of double layer FSS," *IEE Proc.-Microw. Antennas Propag.*, vol. 143, no. 2, pp. 157–162, Apr. 1996.

[35] K. Konstantinidis, A. P. Feresidis, and P. S. Hall, "Broadband sub-wavelength profile high-gain antennas based on multi-layer metasurfaces," *IEEE Trans. Antennas Propag.*, vol. 63, no. 1, pp. 423–427, Jan. 2015.

Marina Mavridou was born in Thessaloniki, Greece, in 1985. She received the B.Sc. degree in physics and the M.Sc. degree in electronics physics from the Aristotle University of Thessaloniki, Thessaloniki, in 2007 and 2010, respectively, and the Ph.D. degree in electronic, electrical, and systems engineering from the University of Birmingham, Birmingham, U.K.

Her current research interests include analysis and design of tunable artificial periodic metamaterials, electromagnetic band gap structures and frequency selective surfaces, as well as tunable microwave and millimeter-wave antennas.

Alexandros P. Feresidis (S'98–M'01–SM'08) was born in Thessaloniki, Greece, in 1975. He received the B.Sc. degree in physics from the Aristotle University of Thessaloniki, Thessaloniki, in 1997, the M.Sc. (Eng.) degree in radio communications and high frequency engineering from the University of Leeds, Leeds, U.K., in 1998, and the Ph.D. degree in electronic and electrical engineering from Loughborough University, Loughborough, U.K., in 2002.

He was initially a Research Associate with Loughborough University in 2002, and then was appointed as a Lecturer in Wireless Communications with the Department of Electronic and Electrical Engineering, where he was promoted to Senior Lecturer in 2006. In 2011, he joined the School of Electronic, Electrical, and Computer Engineering, University of Birmingham, Birmingham, U.K., as a Senior Lecturer. He has authored more than 130 papers in peer-reviewed international journals and conference proceedings and has co-authored three book chapters. His current research interests include analysis and design of metamaterials, electromagnetic band gap structures and frequency selective surfaces, leaky-wave antennas, small/compact antennas, passive microwave/mm-wave/THz circuits, microfabrication, and numerical techniques for electromagnetics and bioelectromagnetics.

Dr. Feresidis is a member of the U.K. EPSRC Peer Review College and is on the Editorial Board of *IET Microwaves, Antennas, and Propagation* journal. He was a recipient of the Senior Research Fellowship Award from the U.K. Royal Academy of Engineering and The Leverhulme Trust (2013–2014).